Determination of buoyancy frequency in weakly stable waters

Hans van Haren[1] and Claude Millot[2]

Received 19 May 2005; revised 26 August 2005; accepted 16 December 2005; published 23 March 2006.

[1] Sea-Bird 911(plus) conductivity-temperature-depth (CTD) data are scrutinized for the determination of the buoyancy frequency N in deep (Mediterranean Sea) waters, where N is very small (O(f)), f is the inertial frequency. Precise knowledge of such low stability values is imperative for the understanding of inertio-gravity wave propagation in the ocean. In this paper, truly homogeneous layers that are neutral in stability, N = 0, are not just detected by computing N(z) over a particular pressure window Δp, as such N includes errors due to mismatches of all sensors, but foremost by inspecting individual profiles of directly measured quantities, like temperature T and its variance change with respect to the adiabatic lapse rate Γ. Depending on the size of Δp, neutral stability can be computed in the deep layer of homogeneous water to within an error of $\sim$0.8f (using Δp = 100 dbar) and $\sim$0.4f (Δp = 600 dbar). The latter error is about half due to the imprecise measurement of Γ due to poor resolution of the T sensor. The former error is largely due to the (in)accuracy of individual sensors of the CTD and/or their imperfect measurement of dynamical heterogeneity in T and salinity S due to mismatch in sensor response time. This heterogeneity in T and S can be more abundant in stratified waters, where it seems more difficult to detect the appropriate value of nonzero but small N. This is fully attributable to the problem of variable length scales of stability motions that are supported by the stratification, while modifying it.

Citation: van Haren, H., and C. Millot (2006), Determination of buoyancy frequency in weakly stable waters, *J. Geophys. Res.*, *111*, C03014, doi:10.1029/2005JC003065.

1. Introduction

[2] As outlined by, e.g., *Wunsch and Webb* [1979], a key problem in studies on internal wave motions in the ocean has been the precise determination of the buoyancy frequency $N = (-g\,d\ln\rho/dz)^{1/2}$, g the acceleration of gravity, that describes the stability of a water column in terms of density (ρ) variations experienced by a water parcel displaced across a vertical distance Δz, or in terms of pressure: Δp. Hence N is the upper frequency limit of freely propagating internal gravity waves. In the open ocean, density is a function of temperature, salinity and pressure so that, in theory, N(z) can be determined from a vertical profile of these three quantities. At the time however, the quality of data of salinity (conductivity) and temperature with depth (CTD) was considered relatively limited, so that *Wunsch and Webb* [1979] assumed they could not establish N better than to within a factor of $\sim$2.

[3] We consider present-day CTD data to have a quality that is just slightly higher than historic ones. Even though modern equipment more robustly performs than previously, the precise determination of N remains a challenge, simply because of specific problems with the instrumentation and because of the difficulty of choosing Δz due to the spatial and temporal variabilities of N = N(x, y, z, t) in association with internal wave scales mainly, as will become clear below. To circumvent this problem, N is generally determined in a given region by averaging (many) CTD profiles over relatively large vertical distances O(100 m), without specifying such distances. This may give a reasonable estimate of the large-scale background N only. In the remainder of the paper, we will not address the dependence of N on neither x nor y; dependence on t will be only marginally mentioned. Because we mainly focus on the dependence on z of all parameters from CTD vertical profiles, we avoid specifying (z) for N thereafter.

[4] On the basis of open ocean CTD data, the internal gravity wave spectrum was originally scaled by *Garrett and Munk* [1972] (hereinafter GM) in the frequency (σ) range $f < \sigma < N$, f denoting the inertial frequency and N computed from the overall fit of actual profiles to an exponential one, by $P(\sigma) \propto N$, to within the aforementioned factor of 2 [*Fofonoff and Webster*, 1971; GM]. In that case, it may well be that (in)accuracy is not due mainly to the quality of the historic observations, but rather due to the intrinsic property of ocean motions.

[5] During our [*van Haren and Millot*, 2004] recent studies on deep inertial motions and internal waves in the Algerian Basin in the south of the western Mediterranean Sea (Figure 1) we found intermediate and deep layers that distinctly differed from each other in stratification, and special attention is given here to CTD profiles evidencing a nearly homogeneous deep layer in which potential density changes with depth seem to become negligible

[1] Royal Netherlands Institute for Sea Research, Den Burg, Netherlands.
[2] Antenne Laboratoire d'Océanographie et de Biogéochimie, CNRS, La Seyne-sur-Mer, France.

0148-0227/06/2005JC003065$09.00

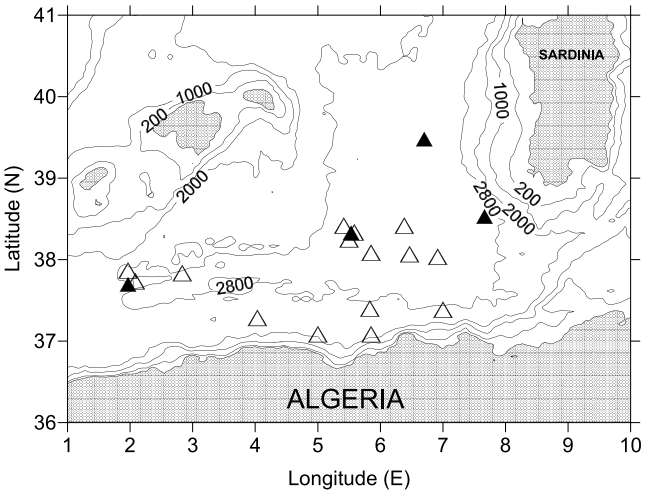

Figure 1. Algerian Basin with stations deeper than 1000 m included: ELISA (July 1997 and March 1998), BADE (October 2003), and GYROSCOP (September 2004). From each cruise, representative data (black triangle stations) are used here.

(Figure 2). The western Mediterranean Sea is one of the few areas where surface water is densified so much that it can sink down to the deep in winter, with associated convection and large vertical motions resulting in a deep "homogeneous" layer of weak if not neutral stability. Figure 2 illustrates the interannual variability where the densest waters accumulate. In such a layer, the sole internal waves that are theoretically able to propagate freely are the gyroscopic waves, of which motions at the inertial frequency can be markedly inclined to the vertical. The recent observation of such gyroscopic waves [*van Haren and Millot*, 2004] thereby requires a determination of stability as precise as possible.

[6] Here, in an attempt to estimate N in layers of weak stability (N $\sim$ 0) and to investigate what variability one can expect, we perform some exercises using several relatively clear-cut modern CTD data sets. Examples are chosen to achieve reasonable diversity: from cruises in different years, from stations spread through the Algerian Basin, provided water depth is greater than 2500 m (to have the deep homogeneous layer thick enough), from three different SBE-911(plus) CTD systems with sensors of the same make, but with different calibrations. For the present analysis, N will be computed following complete preanalysis

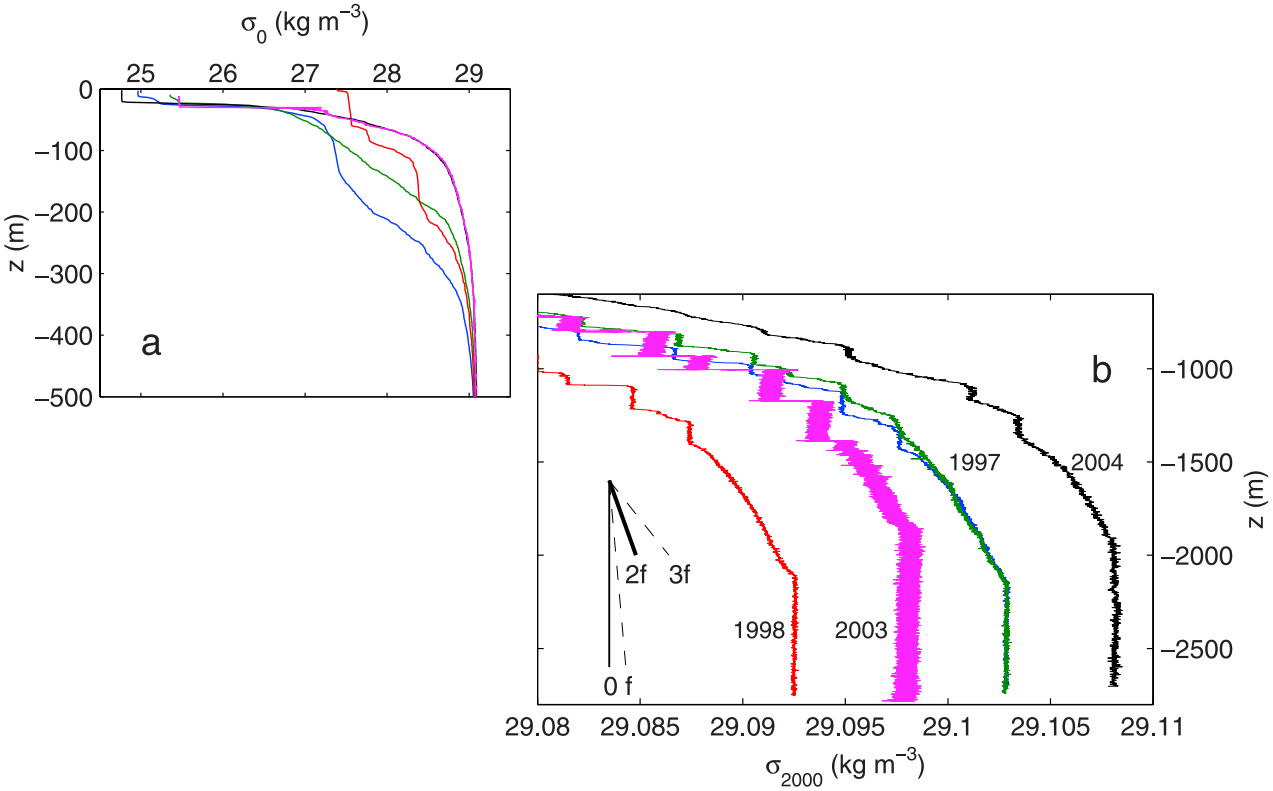

Figure 2. Four examples of 1-m vertical bin averaged density anomaly versus depth profiles obtained in the Algerian Basin (Table 1) in July 1997, March 1998, and September 2004. For comparison, the purple profile shows untreated 24-Hz data in October 2003. (a) Upper 500 m showing potential density anomaly referenced to the surface (ρ_0 − 1000 kg m^{-3}, the black profile is partially masked by the purple one). (b) Data for 500–2700 m showing potential density anomaly that is referenced to 2000 m (ρ_{2000} − 1008.650 kg m^{-3}). Note that the green profile masks the blue one at the deeper levels, which evidences the CTD accuracy. The short sloping lines indicate density stratification yielding N = f, 3f (dashed lines) and N = 0, 2f (solid lines).

Table 1. Positions of Typical (Arbitrarily Chosen) Sea-Bird SBE 911(plus) CTD Stations in the Western Mediterranean Sea[a]

Project	Ship	Period	Latitude, Longitude	Water Depth, m	Number of CTD
ELISA	R/V *Suroît*	Jul 1997	38°20′N, 05°30′E	2734	9
	(R/V *Suroît*	Jul 1997	38°05′N, 06°00′E	2703	Figure 2 only)
	R/V *Suroît*	Mar 1998	39°30′N, 06°45′E	2791	6
BADE	R/V *Pelagia*	Oct 2003	37°40′N, 02°00′E	2731	4
GYROSCOP	R/V *Thethys II*	Sep 2004	38°30′N, 07°40′E	2800	1

[a]Number of CTD indicates the number of deep CTD casts (deeper than 2500 m) during a particular campaign, from each of which one a typical station is chosen. Two profiles are chosen from the 1997 campaign.

treatment of the data. Errors in such N(z) will be compared with errors in detecting homogeneous layers in profiles of individual sensors that require as little as possible preanalysis treatment. As will be demonstrated, in some cases raw untreated data are best for the analysis. First however, we consider basic formulations of N.

2. Determination of Stability

[7] As can be found in the work of Fofonoff [e.g., *Bray and Fofonoff*, 1981; *Fofonoff*, 1985] and in several textbooks [e.g., *Gill*, 1982; *Pond and Pickard*, 1986], the in situ static density $\rho_s(z)$ obviously continuously increases with depth. However, temperature increases with pressure in accordance with the adiabatic lapse rate, which prevents easy recognition of a given homogeneous water mass. Introducing ''potential'' quantities, i.e., quantities that would be obtained when adiabatically moving water particles to a given level (be it the surface or any other level) allows resolving this identification problem.

[8] Although the vertical profile of potential density classically referenced to the surface $\rho_0(z)$ indicates better than a static density profile that ocean stability is weak at great depths, its vertical gradient is not an exact measure for stability,

$$N^2 \neq -\frac{g}{\rho_s}\frac{d\rho_0}{dz}, \tag{1}$$

and one should consider a more nearby reference level. For example, in the Channel of Sardinia, where warmer saline waters overlay much cooler and fresher waters, potential density values at 2000 m are lower than at 1500 m when referenced to the surface, while profiles are stable when referenced to ~1750 m. This is because the pressure effect on the changes in density is a nonlinear function of temperature. In other words, the stability of vertical motions depends on the local infinitesimal changes in density $\delta\rho$ of a water parcel when displaced across an infinitesimal vertical distance δz in a static environment that changes between $\rho_s(z)$ and $\rho_s(z - \delta z)$. Thus one requires adiabatic leveling [*Bray and Fofonoff*, 1981] and local (i.e., at z whatever $\delta\rho$ or δp, or in practice over finite intervals Δp (or Δz) static stability occurs when $N^2 > 0$, with

$$N(z)^2 = -\frac{g}{\rho_s}\left\{\frac{d\rho_s}{dz} - \frac{\delta\rho}{\delta z}\right\}. \tag{2}$$

[9] Without deriving we pose the analytically equal but numerical more feasible result [e.g., *Gill*, 1982; *Pond and Pickard*, 1986],

$$N(z)^2 = -\frac{g}{\rho_s}\left\{\frac{d\rho_s}{dz} + \frac{\rho_s g}{c^2}\right\}, \tag{3}$$

where c denotes the local speed of sound and which describes the thermodynamic change in density due to a change in pressure. A numerically more attractive thermodynamic equivalent to (2) and (3) with reference to pressure instead of depth variations is used by *Bray and Fofonoff* [1981] and in Sea-Bird software. As density is not observed via a single sensor, we need another equivalent to (2) and (3) in which directly measurable quantities occur.

[10] In terms of observable static state distributions of in situ temperature $T = T_s(z)$ and salinity $S = S_s(z)$, S derived from observed conductivity $C = C_s(z)$, T and pressure (P), stability can also be written as [e.g., *Sverdrup et al.*, 1946; *Gill*, 1982; *Pond and Pickard*, 1986]

$$N(z)^2 = g\left\{\alpha\left(\frac{dT}{dz} + \frac{\alpha T g}{c_p}\right) - \beta\frac{dS}{dz}\right\}, \tag{4}$$

in which $\alpha = -\rho^{-1}\partial\rho/\partial T$ and $\beta = \rho^{-1}\partial\rho/\partial S$ denote expansion coefficients and c_p the specific heat at constant pressure. The second term on the right hand side of (4) involves the adiabatic lapse rate $\Gamma = \alpha T g/c_p$, which implies that in the ocean where stability is small, and assuming salinity variations are negligible, temperature should increase with depth (with the exception of fresh, cold water where $\Gamma < 0$ [*McDougall and Feistel*, 2003]). In the western Mediterranean Sea, $dT/dz < 0$ occurs at depths where $N < 6f$ (for Γ at ~286 K). It is noted that in (4), temperature should be given in Kelvin not Celsius. Although (4) can be expressed in terms of potential temperature θ, we here investigate vertical gradients of T(z), a single sensor, as θ is computed from data from more than one sensor.

3. Data

[11] During campaigns in 1997, 1998, 2003 and 2004 out of O(100) Sea-Bird SBE-911(plus) CTD profiles ~20 (Figure 1 and Table 1) ranging the entire water column over depths of ~2800 m were obtained in the Algerian Basin at a mean latitude corresponding to $f \approx 1.25$ cpd (cycles per day, 1 cpd = $2\pi/86400$ s^{-1}). P, T and C data were sampled at a rate of 24 Hz while the average descent/ascent speed was 1 ± 0.25 m s^{-1}. The most

recent downcast (the black profile in Figure 2) will be mainly used here. Its upcast and some other downcasts will be used for discussion.

[12] Generally, the sensors are mounted at the bottom of the CTD package, leading to a more or less unobstructed "view" of the water to be sampled during the downcast, which implies an expected enhanced noise level during the upcast. Problems occur due to the different response times of the sensors (the T sensor is ~1 s slower that the others) and to a varying speed of the CTD through the water column. Hence, in a SBE-911(plus) the C and T sensors are mounted in a duct through which the water is pumped at a constant rate. In this way, the water flows passed the sensors at a rate that is independent of the motion of the CTD. Additional sensor response mismatch can be compensated during preanalysis treatment of the data. It is noted however that not all different sensor setups could be retraced, resulting in occasional differences in observed instrumental noise.

[13] Prior to analysis, the data are treated using a standard procedure for possible errors due to mismatches in sensors response times, thermal mass (which is a severe problem making this CTD less suitable for resolving fine structure in T and S [*Lueck and Picklo*, 1990]), depth inversions and sensors having different time constants before quantities like salinity and potential density are derived (Tables 2a and 2b; for more details, see the Sea-Bird data processing manual). Here, this treatment is done using the settings in the Sea-Bird data treatment software, which involves some mild low-pass filtering, conductivity cell thermal mass correction and loop editing for wave compensation. No further corrections are applied. Apart from block averaging over 1-m intervals, no further smoothing is used. Especially the application of a median filter should be avoided, as it may hamper the proper determination of N in weakly stable layers. During the analysis of stability in near-neutral waters, also completely untreated data turned out to contain additional useful information, as will be shown using the example of raw 24 Hz data.

[14] After the preanalysis treatment, $N^2(z)$ is computed using Sea-Bird software following the adiabatic leveling method [*Bray and Fofonoff*, 1981] over 25-dbar pressure intervals and subsequently over larger intervals to reduce noise and to search for possibly more appropriate intervals. Although N^2 is computed at pressure levels over a certain window in pressure, with units in dbar, profiles (also for other quantities) will be graphically shown with respect to depth, vertical coordinate z and units in m. As we are investigating N in weakly stratified waters with interest in internal wave ranges, we will express weak N and its accuracy in terms of f.

[15] Using data from individual sensors that are very accurate for general purposes (Tables 2a and 2b), one can compute errors in N on the basis of individual sensors errors, using the terms in (4) separately for T and C (actually S, of course). For fixed S, the accuracy in T of ±0.001 °C using a window of 2400 data points (~100 dbar) would yield a theoretical accuracy in N of $\Delta N = \pm 0.38f$. For fixed T, the accuracy in S using the same window would yield a theoretical $\Delta N = \pm 1.3f$. These expected limit values will be compared with the observations.

Table 2a. Characteristics of Sensors and Raw Data Treatment Using Sea-Bird's Data Treatment Program to Convert the Original 24 Hz SBE 911(plus) 2004 Data[a]

Sensor	Type	Resolution	Initial Accuracy
Temperature, °C	SBE 3plus	0.0003	0.001
Conductivity, S/m	SBE 4	0.00004	0.0003
Pressure, dbar	Paroscientific Digiquartz	0.06	0.9
Salinity,[b] psu	–	~0.00006	~0.0005

[a]Most recent calibration was on 2 October 2003.
[b]Values for salinity are computed from manufacturer's values of other parameters for typical temperature and pressure.

Table 2b. Treatment

Program	Parameters
Filter	A, not used; B, 0.15 s
Align CTD	T, 0.0 s C, 0.0 s
Cell tm	$\alpha = 0.03$, $\tau = 0.07$
Loop edit	minimum velocity 0.25 m/s
Derive	S, σ_0, σ_{2000}, etc.
Bin average	1 m
Buoyancy	Δp, 25–300 dbar

4. Observations

4.1. General

[16] The similarities and differences between the different profiles are visible in the potential density anomalies referred to the surface (Figure 2a) and 2000 dbar (Figure 2b). A seasonal pycnocline is found around 30 m and large variations in density permanently occur between 100 and 300 m (the actual range of the depth of the interface between waters recently entered from the Atlantic and Mediterranean waters). Between 700 and 1500 m, a series of steps (due to double diffusion between warm salty waters originating from the eastern Mediterranean Sea and cooler, fresher and denser waters from the western Mediterranean Sea) is found that have thickness between 50 and 200 m. Between 1500 and ~2000 m, the slope in density anomaly is weak but steady before dropping off suddenly below ~2000 m to near zero in a deep layer ~700 m thick (filling the entire deeper part of the Algerian Basin down to ~2900 m). However, the latter transition is found at depths varying between 2100–2200 m in 1997/1998 and ~1900 m in 2003–2004. It is noted that 1900 m reflects the maximum height of the deep layer trapped in the Algerian Basin as it is the maximum water depth of the sill in the Channel of Sardinia (water in excess will outflow).

[17] Even though T and S do continuously increase with time in the deep layer (*Béthoux et al.*, 1990; for T see Figure 5a in section 4.4), the density anomaly does not show any trend and spreads in a ~0.016 kg m^{-3} range. As will be shown, this density spreading is mainly due to the T and S decadal trends, partially to some interannual variability and, to a very small extent, to sensor misalignment.

4.2. Potential Density Versus Density Referenced to an Arbitrary Level and Detection of N = 0

[18] Before investigating the computed N(z), we consider the differences in slopes in profiles of computed potential density anomaly referenced to the surface

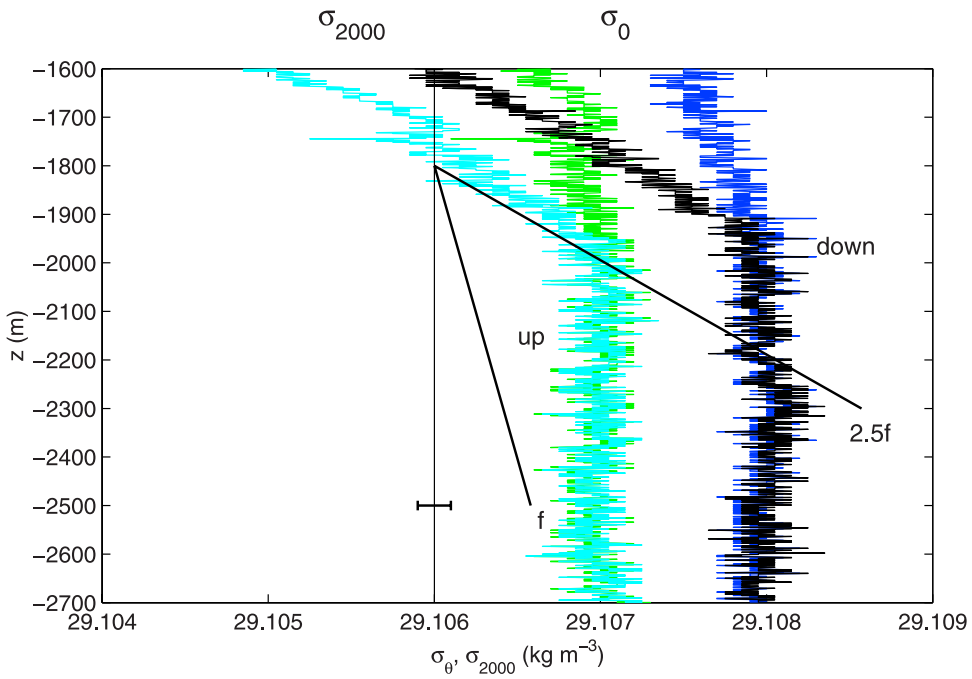

Figure 3. Density anomaly profiles in very weak stratification from upcast and downcast in September 2004 (the black one in Figure 2), demonstrating the difference between surface potential density -1000.0 kg m^{-3} (blue, downcast; green, upcast) and one referenced to 2000 m ρ_{2000} -1008.65015 kg m^{-3} (black, downcast; light blue, upcast). The upcast profiles are arbitrarily off-set to differ by -0.001 kg m^{-3} from the downcast ones. The instrumental noise level is indicated by the error bar.

$\sigma_0 = \rho_0 - 1000$ kg m^{-3} (arbitrary reference density) in comparison with a profile of $\sigma_{2000} = \rho_{2000} - 1008.650$ kg m^{-3} (arbitrary reference density chosen to have both plots fitted in a single frame) in the middle of the weakly stratified layer of interest (Figure 3). These profiles are also representative of other profiles of quantities like $\theta(z)$ and $S(z)$ that have been computed from data of more than one of the CTD sensors and which also show no vertical gradients when perfectly performing in homogeneous layers. In Figure 3, downcast and upcast of the 2004 profile are included, for comparison. Although we note an offset between the downcast and upcast profiles of $\sim$0.0007 kg m^{-3}, probably due to misalignment of the sensors that could not be corrected using standard post-processing, this was not further investigated here. For clarity the profiles are offset by an arbitrary value.

[19] Above $\sim$1900 m, the slopes of profiles referred to either 0 or 2000 m differ greatly, thus reflecting heterogeneous waters which expresses the aforementioned notion that the gradient of potential density is not an exact measure for stability. Naturally, the slope in σ_{2000} yields an exact solution for N only around 2000 dbar (and the slope in σ_0 cannot yield an exact solution for N at that position), but within the range between 1600 and 1900 m half of the deviation between σ_{2000} and σ_{1600} is equivalent to the instrumental noise level of $\sim 10^{-4}$ kg m^{-3}.

[20] Below $\sim$1950 m, the slope is indistinguishable between σ_{2000} and σ_0 in both the upcast and downcast, which is an indication of a unique water mass that has been adiabatically transported from the surface down to these depths, hence following (2) one expects neutral N = 0.

[21] This is best verified by computing the slope in the profiles between 1950 and 2700 m in Figure 3, which is $\sim 1 \pm 1 \times 10^{-4}$ kg m^{-3} over this depth interval, which is equivalent to N = 0.4 ± 0.4f and thus significantly less than N = f (Figure 3). The apparent weak slope in the downcast between 2180 and 2250 m is equivalent to N $\sim$ f locally, but it may be due to an instrumental error as it is not visible in the upcast. It is noted that, in such a homogeneous layer, the error in the determination of a slope in potential density is partially caused by the instrumental noise and partially by natural heterogeneity, which precludes the determination of N < 2f over small pressure windows ($\Delta p < 25$ dbar) to within a statistically significant level, or the apparent distinction between weakly stable and near-neutral layers.

4.3. Computing N for Different Pressure Intervals in Varying Stratification

[22] When N(z) is computed over an interval of 25 dbar to within an expected error of $\sim$2.5f (section 3), one notes (Figure 4a) a smooth N profile from the surface down to $\sim$700 m and a roll-off to an apparent "minimum" level of, indeed, 2–2.5f below 1500 m. In between these transition depths, regularly large variations are found, including unstable overturns and homogeneous layers, which are associated with the O(100 m) thick layers that are related to double diffusive processes. Below 1500 m, the profile appears blurred due to the many unstable layers, which is not commensurate to the clear-cut density profiles in Figure 3. To avoid the inclusion of instability in the computation of N, one possibility is to enlarge the pressure interval.

[23] Using $\Delta p = 100$ dbar (Figure 4b), with an expected noise limitation of $\Delta N \sim 1.3f$, some of the layering between 700 and 1500 m is still clearly visible, although the uppermost layer of weak N (near 900 m) no longer shows N < f: some of the (expected) neutrally stable layers had vertical length scales smaller than $\sim$100 m. Between 1500

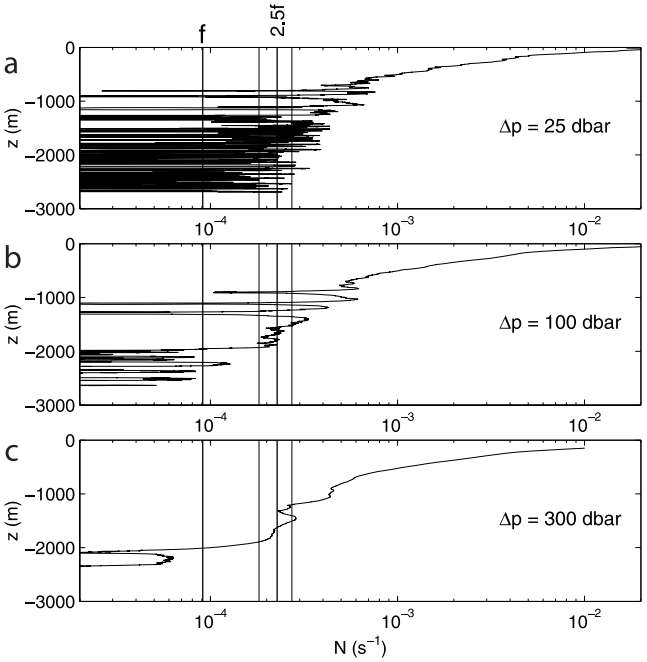

Figure 4. N computed for different vertical windows using downcast of the entire profile obtained in September 2004.

and 1900 m, N is stable and remarkably uniform around N = 2.5 ± 0.5f, with a weak tendency to decrease with depth. The sudden transition at ∼1900 m in Figure 3 is now also clearly visible. Below ∼2000 m, N < f, but computed N is still often unstable, except between 2200 and 2250 m, which shows a small layer of apparent N = 1−1.5f (this layer is not visible in the upcast profile).

[24] In the N profiles smoothed over Δp = 300 dbar (Figure 4c), with an expected noise limitation of ΔN ∼ 0.6f, no neutral layers are found above 1500 m, these are all smoothed away. In the layer below 2000 m most stability is at or below noise level, but it is noted that in this layer one instability is still visible, and further smoothing would be in fact necessary to remove them all (as can done using a method suggested by *Jackett and McDougall* [1995]). We conclude that, with a relatively large-scale (300 dbar) smoothing, there is still a layer of neutral stability in the deep western Mediterranean Sea, with an error better than the ΔN ∼ 0.6f due to the instrumentation.

[25] However, it may be better to investigate profiles of individual sensor quantities, especially for finding layers of O(100 m) or less vertical extent, since more accurate, stable density (N) matched ''sensors'' are presently not marketed. We start with investigating profiles of T(z) and it is hypothesized that perhaps the most precise manner to determine neutral stability is by considering (the high-frequency noise in) the slope of in situ temperature T(z), not of potential temperature θ(z), (referenced to the surface). Profiles of T(z) are special as for neutral N they still show a vertical gradient, which is dependent on the value of local temperature in Γ.

4.4. T(z)

[26] As a measure for high-frequency variations in T(z), we computed the standard deviation std(T) of portions of detrended T (over a 100-dbar interval). This interval is chosen because it is of the same size as the average step layer and, with hindsight, the associated error in N is mostly limited by instrumental noise in T rather than a mismeasured adiabatic lapse rate, as will be demonstrated later in this section. Of course, ideally one wants an even smaller interval, but that requires much more accurate sensors.

[27] The downcast profiles of T(z) (Figure 5a) and std(T)(z) (Figure 5b), obviously also evidence the aforementioned sharp transition near ∼1950 m in the 2004 (black) data (∼1850 m for purple (2003 data) and ∼2200 m for green, blue and red profiles (1997–1998 data)). This transition is visible in T(z) as its slope becomes near constant with depth in the deep, approaching the value of local Γ (light blue), but it is more clearly visible in the drop in high-frequency variations for depths greater than the transition depth. Figure 5a accounts for a unique water mass in which T varies only due to compression [*McDougall and Feistel*, 2003], and clearly evidences the noise (both instrumental and actual) in that layer. The drop in std(T) at a transition depth suggests a sudden change in hydrography (water masses), and possibly also a change from internal gravity wave activity and/or vertical turbulent diapycnal exchange to instrumental noise levels and homogeneity: this clearly marks a transition in motions between the deep layer (WMDW: homogeneous, formed nearby in the Gulf of Lions) and the layer above (TDW: stratified resulting from exchange between WMDW and waters from the eastern Mediterranean Sea). It is noted that high-frequency variations in the deep are not only instrumental since even an ''homogeneous'' layer is heterogeneous at small scales, but levels do approach instrumental noise estimates.

[28] The temperature of the deep water, i.e., below the transition depth, changes with time. The 2003–2004 data are warmer than the 1997–1998 ones by ∼0.027 °C, which has to be compared with the long-term trend of 0.03°C/decade that has been evidenced for this water where it is formed [*Béthoux et al.*, 1990]. This discrepancy may partially be due to the different sampling locations, that is horizontal heterogeneity, and/or to interannual variability. This heterogeneity may affect the observed different high-frequency temperature noise levels, in addition to instrumental causes due to different set-ups. The 1997–1998 noise is 0.5–0.7 times the 2003–2004 one. By the same token, the 1-m binned 2003 data have a 100-dbar interval noise level larger than those of 2004 by a factor of 1.3–1.5. It is noted that for the 2003 data the depth of transition to higher noise levels is equally well found using the raw data (purple graphs, not scaled by Δp) instead of 100 dbar smoothed data.

[29] Using std(T), the layer below ∼2000 m is estimated homogeneous to within a high-frequency noise of ∼0.8 × 10^{-4} °C (over an interval of 100 dbar) for the observed downcast profile. However, also the estimate based on the manufacturer's accuracy, which has nearly the same value, is a theoretical lower limit estimate, as it does not include the imperfect measurement of the adiabatic lapse. This is investigated using raw data.

4.5. Measuring Γ Using Raw Data

[30] The raw 2003 data yield high-frequency noise levels that are very close to the manufacturer's noise level, which

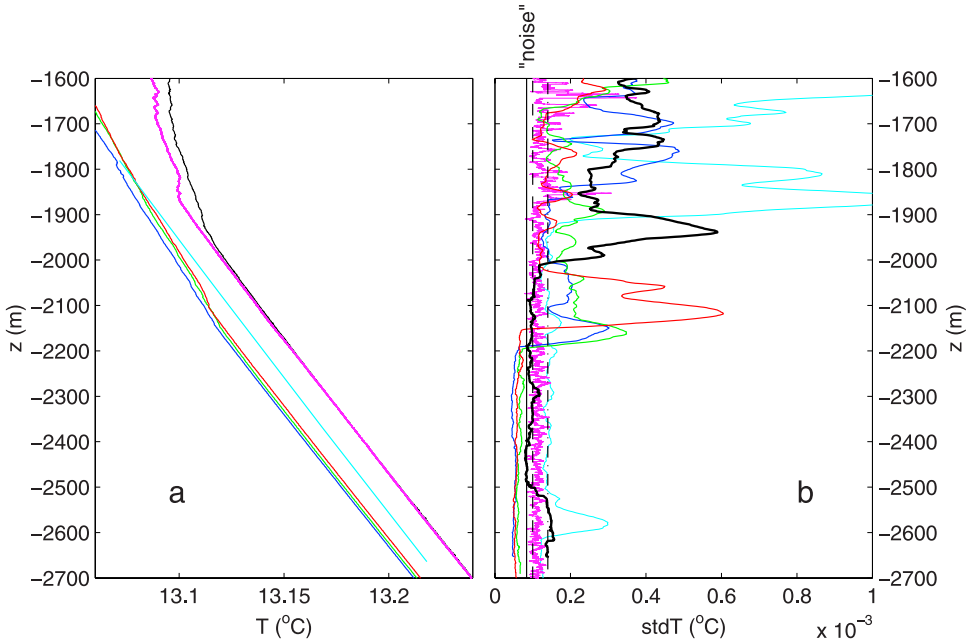

Figure 5. (a) Temperature in very weak stratification for downcast of 1-m averaged CTD profiles obtained in September 2004 (black), in July 1997 (blue, green), and March 1998 (red), and with the untreated 24 Hz 2003 data (purple). The adiabatic lapse rate is in light blue. (b) Standard deviation of detrended portions of 100 data points (~100 dbar; for the 24 Hz data ~4 dbar in purple and 2400 data points or ~100 dbar in light blue) using the profiles in Figure 5a. The solid line is the "initial accuracy" given by the manufacturer and divided by $2400^{1/2}$ that is very close (to within 15%) to the expected error including the error introduced by erroneously estimating the adiabatic lapse rate (dashed line). The manufacturer's accuracy for the 24-Hz data is given by the dot-dashed line.

amounts 10^{-4} °C = 10^{-3} °C/$\sqrt{100}$ data points, using an interval of ~4 dbar (Figure 5b). However, we note that this noise level is quite coincidental here, as it displays the limitation of T measurement resolution (Figure 6): the zig-zag pattern in Figure 6b evidences the attempted measurement of Γ using a resolution that is twice as large (~3×10^{-4} °C m^{-1}).

[31] The local $\Gamma \approx 1.7 \times 10^{-4}$ °C m^{-1}, and its rate of change is approximately $d\Gamma/dz \approx 1.1 \times 10^{-8}$ °C m^{-2} (Table 3). As a result, the error in the mean temperature

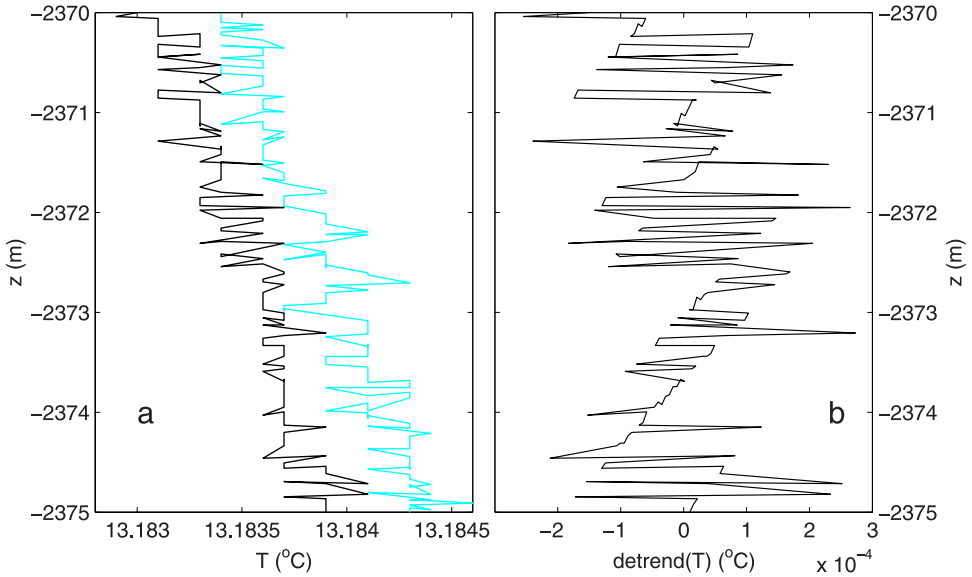

Figure 6. Effect of measuring the adiabatic lapse rate of ~1.7×10^{-4} °C m^{-1} with a sensor that has a resolution of ~3×10^{-4} °C, using the 24 Hz untreated 2003 data over 5 m in the deep near-neutral layer. (a) Observed temperature profile for upcast (light blue) and downcast (black). (b) Detrended downcast profile, which shows a mean standard deviation of ~1.1×10^{-4} °C.

Table 3. Estimates (Γ_{obs}) of Adiabatic Lapse Rate Γ[a]

Reference Pressure, dbar	Γ_{th}, 10^{-4} °C m^{-1}	Γ_{obs}, 10^{-4} °C m^{-1}	$\Gamma_{obs} - \Gamma_{th}$, 10^{-6} °C m^{-1}
2000	1.628	1.594	−3.4
2100	1.639	1.573	−6.6
2400	1.671	1.642	−2.9
2700	1.703	1.703	−0.0

[a]Using 20 m intervals of raw, uncorrected 24 Hz CTD observations obtained in the weakly stable (about neutral) deep layer below ~2000 m in September 2003, as compared with *Feistel and Hagen*'s [1995] "theoretical" Γ_{th}. The estimated mean error in the lapse rate inferred from observations is than 3.2×10^{-6} °C m^{-1}.

averaged over 24 data points (~1 dbar) is not 2×10^{-4} °C as expected from instrumental noise, but 2.6×10^{-4} °C, due to the poor resolution, in an area where temperature is exclusively determined by Γ. Furthermore, as the change $\Delta\Gamma \approx 8.2 \times 10^{-6}$ °C over 750 dbar, we cannot estimate N better than about $\Delta N \sim 0.45$ f from temperature alone using a linear gradient. Thus the "theoretical" value computed in section 2 from instrumental noise is nearly doubled, because of the imperfect estimate of the (curvature in) adiabatic lapse rate using a poorly resolving T sensor. This value can only be improved by considering smaller window sizes, but then one needs more accurate sensors. For a window of 100 dbar the portion in the error due to a mismeasurement of $d\Gamma/dz$ is negligible, and we find $\Delta N \sim 0.85$ f, compared to 0.76 f for instrumental noise alone. These values are marginally smaller than found in section 4.3 using N computed from completely corrected data from different sensors. However, for the detection of neutral layers the use of T(z) seems suitable, as also smaller window sizes can be used down to O(1 dbar). The remaining question is whether such small sizes are also needed for estimating N in weakly stratified layers $N > 0$. This will be discussed in section 5.

4.6. C(z)

[32] The deep 2004 conductivity record is investigated (Figure 7) in a similar manner as the temperature record in Figure 5. As with the latter, conductivity attains a near-constant slope and a sudden drop in high-frequency "noise" below 1950–2000 m (the transition depth is nearly the same as using T). As for T, the upcast noise level is about twice that of the downcast, while the latter is approximately 1.5 times the manufacturer's accuracy. As with T, the advantage of inspecting this record is the possibility of detecting layers that have neutral stability using vertical length scales smaller than needed for statistical significance.

5. Discussion

[33] From our observations it seems that present-day (Sea-Bird) CTD observations are capable of detecting layers of neutral stability to within an error better than $\Delta N \sim 0.5$ f, provided a suitable vertical window of about 300 dbar is used. Over this window about a third of this error is due to the imprecise measurement of the adiabatic lapse rate and another quarter due to a mismatch between individual sensors. Alternatively, one can use only temperature (or conductivity) data to detect homogeneous layers (Figure 8). This has the advantage that the window size can be reduced to 100 dbar, or less, and that the data record does not have to be matched to others. However, using T requires knowledge of the adiabatic lapse rate while using T and C requires knowledge of the high wave number footprint of internal waves related to that of instrumental noise.

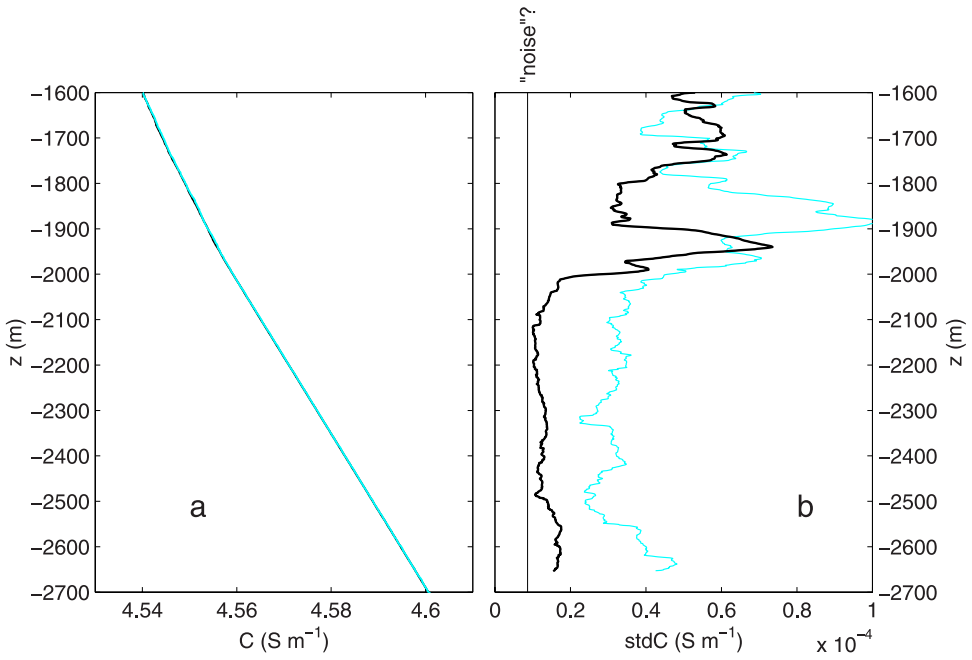

Figure 7. Same as Figure 5 (upcast (light blue) and downcast (black) of the 2004 profile) but for conductivity. In Figure 7b the vertical line indicates error estimated using the manufacturer's accuracy estimate.

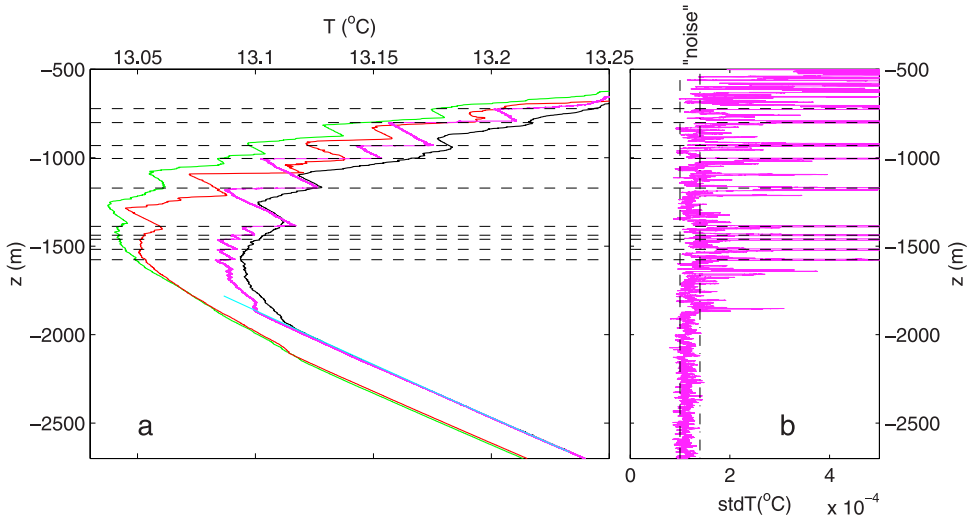

Figure 8. Same as Figure 5 but for a larger depth range to demonstrate the usefulness of considering T(z) and its high-frequency noise in finding near-neutral layers that have vertical length scales of O(100 m) between ~700 and 1500 m. The stratified layers between the steps can be very thin, down to only 1 m in the vertical, and they are used for reference (thin dashed lines) to connect the purple curves in both panels. In Figure 8b, only the purple graph of ~4 dbar windowed data from Figure 5b is given (enlarged).

[34] The results are quite suitable for detecting neutrally stable layers of the corresponding (~100 m) or larger vertical length scale. The statistical uncertainty is below f, which is interesting for studies on reflections of internal gravity waves or on transitions between internal gravity and gyroscopic waves, as suggested by *van Haren and Millot* [2004].

[35] In weakly stable stratified layers however, this length scale of 100 m may be difficult to maintain, as it conflicts with typical scales of internal gravity waves. Using the temperature variance (Figure 5b) as a measure, a typical vertical length scale of the strongly stratified layers is O(1 m), as in Figure 8. A comparison with profiles of downcast and upcast and between different profiles from different stations confirms this variability, but such steps are only smoothed when a very large window is used of several 100 dbar (Figure 4c). In more weakly stratified layers with fewer steps, a smaller window size seems possible. If we then take, for example, a window of 100 dbar and consider the depth range between 1500 and 1900 m, we are able to compute N = 2.5 ± 0.5f. This means that N is determined well within a factor of 2, while the standard deviation is partially determined by the large-scale slope in N.

[36] However, one could also argue that this N is not suitable for studying internal wave motions that have length scales of O(1–10 m), as their "background stratification" has been wiped out by the smoothing over 100-m scales. For these motions, a shorter length scale should be chosen that also handles the background slope within the window well. Inspection of high-frequency temperature variations and differences between the upcast and downcast profiles in the range 1500–1900 m, yields, somewhat arbitrarily, Δp = 25 dbar. Then (Figure 4a), using a SBE 911(plus) CTD the determination of N = 3 ± 1.5f, which means an uncertainty range that is even larger than the factor of two mentioned so often [GM; *Wunsch and Webb*, 1979].

[37] **Acknowledgments.** We thank Gerhard Herndl for obtaining CTD profiles during his BADE-1 cruise, and we thank Jean-Luc Fuda and Gilles Rougier for operating CTD instrumentation during the other cruises. Margriet Hiehle provided Figure 1. We gratefully acknowledge support from the Netherlands Organization for the Advancement of Scientific Research, NWO, and Centre Nationale de la Recherche Scientifique, CNRS, to continue our French-Dutch collaboration.

References

Béthoux, J.-P., B. Gentili, J. Raunet, and D. Tailliez (1990), Warming trend in the western Mediterranean deep water, *Nature*, *347*, 660–662.

Bray, N. A., and N. P. Fofonoff (1981), Available potential energy for MODE eddies, *J. Phys. Oceanogr.*, *11*, 30–47.

Feistel, R., and E. Hagen (1995), On the GIBBS thermodynamic potential of seawater, *Progr. Oceanogr.*, *36*, 249–327.

Fofonoff, N. P. (1985), Physical properties of seawater: A new salinity scale and equation of state for seawater, *J. Geophys. Res.*, *90*, 3332–3342.

Fofonoff, N. P., and F. Webster (1971), Current measurements in the Western Atlantic, *Phil. Trans. R. Soc. London, Ser. A*, *270*, 423–436.

Garrett, C. J. R., and W. H. Munk (1972), Space-time scales of internal waves, *Geophys. Fluid Dyn.*, *3*, 225–264.

Gill, A. E. (1982), *Atmosphere-Ocean Dynamics*, 662 pp., Elsevier, New York.

Jackett, D. R., and T. J. McDougall (1995), Minimal adjustment of hydrographic profiles to achieve static stability, *J. Atmos. Oceanic Technol.*, *12*, 381–389.

Lueck, R., and J. J. Picklo (1990), Thermal inertia of conductivity cells: Observations with a Sea-Bird cell, *J. Atmos. Oceanic Technol.*, *7*, 756–768.

McDougall, T. J., and R. Feistel (2003), What causes the adiabatic lapse rate?, *Deep Sea Res., Part I*, *50*, 1523–1535.

Pond, J. S., and G. L. Pickard (1986), *Introductory Dynamical Oceanography*, 2nd ed., 329 pp., Elsevier, New York.

Sverdrup, H. U., M. W. Johnson, and R. H. Fleming (1946), *The Oceans, Their Physics, Chemistry and General Biology*, 1087 pp., Prentice-Hall, Upper Saddle River, N. J.

van Haren, H., and C. Millot (2004), Rectilinear and circular inertial motions in the western Mediterranean Sea, *Deep Sea Res., Part I*, *51*, 1441–1455.

Wunsch, C., and S. Webb (1979), The climatology of deep ocean internal waves, *J. Phys. Oceanogr.*, *9*, 235–243.

C. Millot, Antenne LOB-COM-CNRS, c/o IFREMER, BP 330, F-83507 La Seyne-sur-mer, France.

H. van Haren, Royal Netherlands Institute for Sea Research (NIOZ), P. O. Box 59, NL-1790 AB Den Burg, Netherlands. (hansvh@nioz.nl)